International Journal of Solids and Structures 45 (2008) 4615–4628

Contents lists available at ScienceDirect

International Journal of Solids and Structures

journal homepage: www.elsevier.com/locate/ijsolstr

Thermoviscoplastic modelling of asymmetric effects for polymers at large strains

R. Mahnken [a,*], A. Shaban [a], H. Potente [b], L. Wilke [b]

[a] University of Paderborn, Chair of Engineering Mechanics, Warburger Str. 100, D-33098 Paderborn, Germany
[b] University of Paderborn, Institute of Plastics, Warburger Str. 100, D-33098 Paderborn, Germany

ARTICLE INFO

Article history:
Received 20 December 2007
Received in revised form 18 March 2008
Available online 2 June 2008

Keywords:
Thermoviscoplasticity
Asymmetric effects
Polymers
Large strains
Numerical integration
Finite elements

ABSTRACT

Glassy polymers such as polycarbonate exhibit different behaviours in different loading scenarios, such as tension and compression. To this end a flow rule is postulated within a thermodynamic consistent framework in a mixed variant formulation and decomposed into a sum of weighted stress mode related quantities. The different stress modes are chosen such that they are accessible to individual examination in the laboratory, where tension and compression are typical examples. The characterisation of the stress modes is obtained in the octahedral plane of the deviatoric stress space in terms of the Lode angle, such that stress mode dependent scalar weighting functions can be constructed. Furthermore the numerical implementation of the constitutive equations into a finite element program is briefly described. In a numerical example, the model is used to simulate the laser transmission welding process.

1. Introduction

The effect of *asymmetry* is an experimental observation for various materials, where the mechanical response is dependent on the loading type such as tension and compression. An example is given e.g. in Spitzig et al. (1975) for a martensitic steel. Concerning the asymmetry effect between tension and compression for polymers, results have been published, e.g., in Spitzig and Richmond (1979) for two different polymer materials (polyethylene and polycarbonate). The yield stress in compression is greater than that in tension (see also Haward et al., 1971 and Section 6.1 of this paper). This observation is labelled also *strength-difference effect* (SD-effect). More details can be found in Spitzig and Richmond (1979). Further examples are presented in Altenbach et al. (1995) for different metallic, polymer and glass fiber-reinforced composite and geomaterials.

In addition the pressure-dependent yield behaviour of several sintered materials and polymers (polypropylene (PP), polycarbonate (PC), polymethylmethacrylate (PMMA), polyvinylchloride (PVC), polystyrene (PS)) including anisotropic effects have been investigated in more detail by Betten (1982a),Betten et al. (1982),Betten and Borrmann (1984). For creep behaviour the SD-phenomenon is called *creep-strength-differential effect* or *CSD-effect* (Betten and Borrmann, 1987). Based upon the *theory of invariants* Kolupaev (2006) has studied CSD-effects of thermoplastics including experiments on polyamide (PA), PC, PS, PVC and PMMA under tension, compression and torsion.

The concept of stress mode dependent weighting functions has been introduced in Mahnken (2003) for simulation of asymmetric effects within a geometrically linear theory and is applied to glassy polymers in Shaban et al. (2007). The key idea here consists in an additive decomposition of the inelastic strain rate tensor. Each of the additive quantities incorporates a *weighting function* dependent on the *stress mode angle* or *Lode angle*, respectively. One advantage of this approach is, that

* Corresponding author. Tel.: +49 5251 602283; fax: +49 5251 603483.
E-mail address: rolf.mahnken@ltm.uni-paderborn.de (R. Mahnken).

0020-7683/$ - see front matter © 2008 Published by Elsevier Ltd.
doi:10.1016/j.ijsolstr.2008.03.033

the chosen stress modes are accessible to individual examination in the laboratory, where tension and compression are typical examples. In this way also certain (though not all) material parameters, such as Norton-type constants, can be identified individually from specific experiments.

To extend the previous concept to include the thermomechanical behaviour within a geometrically nonlinear case, several publications can be found in the literature. Helm (2006) has introduced a constitutive theory in the framework of continuum thermomechanics to represent the viscoplastic behaviour of metals at finite deformations. In particular, the experimentally observed thermomechanical coupling phenomena are described by the theory. Concerning the thermomechanical modelling of glassy polymers at large strains, further literature can be found. Boyce et al. (1988) has developed a constitutive model based on the macromolecular structure of glassy polymers. Using the concept of the previous model, Arruda et al. (1995) studied the effects of strain rate and temperature on the inelastic response of the glassy polymers.

The main purpose of the present work is to extend the concept introduced in Shaban et al. (2007) to the geometrically nonlinear case taking into consideration the thermomechanical effects. To this end a flow rule is postulated within a thermodynamic consistent framework in a mixed variant formulation, which preserves the volumetric and deviatoric properties for the pull-back and push-forward operations. Then, in accordance with the approach of Shaban et al. (2007) an additive decomposition of the flow rule is assumed into a sum of weighted stress mode dependent quantities. Upon performing pull-back and push-forward operations, the flow rule is also formulated with respect to different configurations. In a further part of the paper numerical aspects are addressed. In particular the mixed-variant flow-rule is integrated by an exponential integration scheme, thus leading to a formulation in principal directions and allowing the algorithm developed in Shaban et al. (2007) for the geometrically nonlinear case. The proposed integration scheme can further be implemented into a finite element program such as the UMAT subroutine of the commercial finite element program (ABAQUS-Version 6.5, 2004). Better results are expected using the proposed model in the simulation of the laser transmission welding process.

The structure of the paper is as follows: Section 2 presents a general framework for stress mode dependent thermoviscoplasticity at large strains. In particular a flow rule is postulated in a mixed variant formulation which is decomposed additively into stress mode related quantities. In Section 3 stress mode related weighting functions are introduced briefly, which are incorporated into a prototype model of Section 4. Aspects of the numerical implementation into ABAQUS are briefly described in Section 5. A simulation of the laser transmission welding process is presented in Section 6.

1.1. Notations

Square brackets $[\bullet]$ are used throughout the paper to denote 'function of' in order to distinguish from mathematical groupings with parenthesis $(\bullet)$. Furthermore *tensor calculus on manifolds* as advocated by Marsden and Hughes (1993),van der Giessen and Kollmann (1996) and Hackenberg (1992) is used. In particular rigorous application of the scalar product (*dual pairing*) between co- and contra-variant vectors is employed, thus leading to a concept of simple tensors with unambiguous transformation rules between different vector and tensor spaces. Details on this mathematical formalism are presented, e.g., in Mahnken (2005a) and applied to the framework of multiplicative plasticity, some relevant relations of kinematics are summarised in Appendix A.

2. Framework for stress mode dependent thermoviscoplasticity at large strains

2.1. Kinematics

The constitutive equations used in this work are formulated in the framework of large strain thermoviscoplasticity. To this end an intermediate configuration is introduced as a consequence of the multiplicative decomposition of the deformation gradient

$$\mathbf{F} = \mathbf{F}_e \cdot \mathbf{F}_c, \tag{1}$$

where $\mathbf{F}_e$ and $\mathbf{F}_c$ are the elastic and creep parts, respectively. Basic concepts of tensor calculus on manifolds with applications to this concept are summarised in Appendix A. Here also relevant strain tensors, rate of deformation tensors related to different configurations and the associated pull-back and push-forward operations are summarised. Further details on the concept of multiplicative plasticity with a plastic part instead of a creep part in Eq. (1) can be found in many references, see e.g. Bertram (2005), Haupt (2000), Lee (1969), Miehe (1994), Simo and Hughes (1998), amongst others.

2.2. Entropy inequality principle

Thermodynamic formulations for the constitutive equations are based on the second law of thermodynamics which leads to what is known as the Clausius–Duhem inequality

$$\mathscr{D} = \mathscr{D}_{\text{loc}} + \mathscr{D}_{\text{con}} \geqslant 0, \tag{2}$$

where

$$\mathscr{D}_{\text{loc}} = \frac{1}{\rho_R}\mathscr{P} - \partial_t \Psi - \dot{\vartheta}\eta \tag{3}$$

and

$$\mathscr{D}_{\mathrm{con}} = -\frac{1}{\rho_R \vartheta}\mathbf{q}_R \cdot \mathrm{Grad}\vartheta. \tag{4}$$

Therein $\mathscr{D}$ is the dissipation which is splitted up into two parts $\mathscr{D}_{\mathrm{loc}}$ and $\mathscr{D}_{\mathrm{con}}$. $\mathscr{P}$ is the stress power, Ψ the Helmholtz free energy function, ϑ the absolute temperature, η the entropy, ρ_R the mass density in the reference configuration, $\mathbf{q}_R$ the heat flux vector in the reference configuration, and Grad the material gradient.

A stronger condition of the inequality (2) is introduced by setting both parts greater than zero, which yields

$$\begin{aligned} &1.\ \text{Clausius—Planck inequality} : \mathscr{D}_{\mathrm{loc}} \geqslant 0, \\ &2.\ \text{heat conduction inequality} : \mathscr{D}_{\mathrm{con}} \geqslant 0. \end{aligned} \tag{5}$$

A common approach for the heat flux vector in Eq. (4) is

$$\mathbf{q}_R = \lambda(\det\mathbf{F})\mathbf{C}^{-1}\mathrm{Grad}\vartheta, \tag{6}$$

where $\mathbf{F}$ is the deformation gradient introduced in Eq. (1), λ a non-negative heat conduction coefficient and $\mathbf{C}$ the right Cauchy–Green tensor introduced in Eq. (A.4) in Appendix A.

Several possibilities exist in order to formulate the stress-power $\mathscr{P}$ as a dual-pairing of conjugate stress and strain-rate tensor quantities. E.g., relative to the actual configuration $\mathscr{B}$ it is given as a dual pairing $\mathscr{P} = \boldsymbol{\tau} : \mathbf{d}$ in terms of the Kirchhoff stress tensor $\boldsymbol{\tau}$ and the rate of deformation tensor $\mathbf{d}$ introduced in Eq. (A.6.2) Alternatively the stress power can be defined as $\mathscr{P} = \mathbf{S} : \mathbf{D}$ where the second Pilo-Kirchhoff stress tensor $\mathbf{S} = {}^{*}\Phi^{\flat}[\boldsymbol{\tau}]$ and the rate of deformation tensor $\mathbf{D} = {}^{*}\Phi^{\sharp}[\mathbf{d}]$ is defined in the reference configuration. An elastic pull-back operation renders a formulation for $\mathscr{P}$ relative to the intermediate configuration as $\mathscr{P} = \overline{\mathbf{M}} : \overline{\mathbf{L}}$. Here $\overline{\mathbf{M}} = {}^{*}\Phi'_e[\mathbf{m}] = \mathbf{F}_e^{t} \cdot \mathbf{m} \cdot \mathbf{F}_e^{-t}$ is the Mandel stress tensor in a mixed variant representation, i.e. $\overline{\mathbf{M}} = \overline{T}^{j}_{i}\overline{\mathbf{G}}^{\mathbf{i}} \otimes \overline{\mathbf{G}}_{\mathbf{j}}$ as a consequence of the mixed variant representation for the Kirchhoff stress tensor $\mathbf{m} = \mathbf{g}^{\flat} \cdot \boldsymbol{\tau} = \tau^{j}_{i}\mathbf{g}^{i} \otimes \mathbf{g}_{j}$. Furthermore, $\overline{\mathbf{L}} = {}^{*}\Phi'_e[\mathbf{l}]$ is the velocity gradient introduced in Eq. (A.7.1) related to the intermediate configuration.

Let us assume the functional relationship $\Psi = \Psi[\overline{\mathbf{C}}_e, q, \vartheta] = \Psi^{el}[\overline{\mathbf{C}}_e, \vartheta] + \Psi^{p}[q, \vartheta]$ for the Helmholtz free energy, where $\overline{\mathbf{C}}_e$ is the elastic right Cauchy–Green tensor introduced in Eq. (A.4.1), and q is a *strain-like* internal variable.Consequently, using the additive decomposition Eq. (A.8) and the identity $\partial\Psi/\partial\overline{\mathbf{C}}_e : \dot{\overline{\mathbf{C}}}_e = 2(\overline{\mathbf{C}}_e \cdot \partial\Psi/\partial\overline{\mathbf{C}}_e) : \overline{\mathbf{L}}_e$ the Clausius-Planck inequality (5.1) results into

$$\mathscr{D}_{\mathrm{loc}} = \left(\frac{1}{\rho_R}\overline{\mathbf{M}} - 2\overline{\mathbf{C}}_e \cdot \frac{\partial\Psi}{\partial\overline{\mathbf{C}}_e}\right) : \overline{\mathbf{L}} + 2\overline{\mathbf{C}}_e \cdot \frac{\partial\Psi}{\partial\overline{\mathbf{C}}_e} : \overline{\mathbf{L}}_c - \frac{\partial\Psi}{\partial q}\frac{\partial q}{\partial t} - \left(\eta + \frac{\partial\Psi}{\partial\vartheta}\right)\dot{\vartheta} \geqslant 0. \tag{7}$$

Note that in a more general case q can be replaced by a vector or a tensor of higher order. On defining relations for the Mandel stress tensor $\overline{\mathbf{M}}$, *stress like internal variable* Q and the entropy η as

$$1.\ \overline{\mathbf{M}} = 2\overline{\mathbf{C}}_e \cdot \rho_R\frac{\partial\Psi}{\partial\overline{\mathbf{C}}_e}, \qquad 2.\ Q = \rho_R\frac{\partial\Psi^{p}}{\partial q}, \qquad 3.\ \eta = -\frac{\partial\Psi}{\partial\vartheta} \tag{8}$$

and using the standard argument, that the above relation holds for all processes $\overline{\mathbf{L}}$, the dissipation inequality (7) reduces to

$$\rho_R\mathscr{D}^{\mathrm{red}}_{\mathrm{loc}} = \overline{\mathbf{M}} : \overline{\mathbf{L}}_c - Q\frac{\partial q}{\partial t} \geqslant 0. \tag{9}$$

2.3. Flow rule for asymmetric thermoviscoplasticity

Modelling the evolution of inelastic deformations requires a flow rule for some kinematic quantities, which has been an issue in many publications. In the framework of a geometrically linear theory for creep an extensive overview on different concepts, the potential theory and the tensor function theory, has been published by Betten (2001).

In this work a creep potential theory is applied, although, as noted in Rice (1970), from the physical point of view the assumption of a creep potential has limited justifications. Especially this holds in the anisotropic case and in the tertiary creep stage, Betten (2004). For the plastic potential theory this aspect has been pointed out in more detail in Betten (1985) from the mathematical point of view. As discussed by Betten (1982b) alternatively, constitutive equations can be represented as tensor-valued functions.

The simulation of asymmetric material behaviour is formulated in Shaban et al. (2007) on the basis of a *stress mode* related approach within a geometrically linear theory. The key idea is an additive decomposition of the inelastic strain rate into a sum of stress mode related quantities, which can be investigated individually in the laboratory. In order to extend this approach to the geometrically nonlinear case, in this work a general flow rule is formulated for the creep velocity tensor $\overline{\mathbf{L}}_c$ occurring in Eq. (9) in a nine dimensional space. According to Mahnken (2005b) a non-associated flow rule is postulated:

$$\overline{\mathbf{L}}_c = \sum_{i=1}^{S} w_i\dot{\Lambda}_i\frac{\partial\Phi^{*}_i}{\partial\overline{\mathbf{M}}} \tag{10}$$

i.e. it is formulated as a sum of S individual quantities. The weighting functions w_i are stipulated such that

$$\begin{aligned} &1.\ \sum_{i=1}^{S} w_i[\overline{\mathbf{M}}] = 1 \\ &2.\ w_i[\overline{\mathbf{M}}_j] = \delta_{ij}, \end{aligned} \tag{11}$$

i.e. the weighting functions w_i are associated to different independent characteristic *stress modes* characterised by stress tensors $\overline{\mathbf{M}}_j, j = 1, 2, \ldots, S$. Specific formulations referring to stress states which can be investigated experimentally, e.g. in tension and compression, are given in the ensuing Section 3. We also remark, that Eq. (11.1) can be regarded as a *completeness condition*, whereas Eq. (11.2) constitutes a *normalisation condition* for the weighting functions.

Furthermore, in Eq. (10) $\Phi_i^* = \Phi_i^*[\overline{\mathbf{M}}, Q], i = 1, \ldots, S$ are creep potentials, formulated in terms of the Mandel stress tensor $\overline{\mathbf{M}}$, and internal stress-like variable Q, which appear as the conjugate (dual) variables of $\overline{\mathbf{L}}_c$ and q in the inequality (9). Additionally, in Eq. (10) flow factors are introduced with the functional relationship $\dot{\Lambda}_i = \dot{\Lambda}_i[\overline{\mathbf{M}}, Q]$. In accordance to standard approaches a Norton rule, or in case of power law breakdown, a Garofalo rule (see e.g. Poirier, 1985) is postulated for each flow factor, i.e.

$$1.\ \text{Norton}: \dot{\Lambda}_i = A_i \left(\frac{\langle \Phi \rangle}{\sigma_0} \right)^{m_i}, \quad 2.\ \text{Garofalo}: \dot{\Lambda}_i = K_i (\sinh \alpha_i \langle \Phi \rangle)^{n_i} \tag{12}$$

and where A_i, m_i and K_i, α_i, n_i are material parameters associated to each mode $i = 1, \ldots, S$. Furthermore the notation $\langle \Phi \rangle = x$ for $x > 0, \langle \Phi \rangle = 0$ for $x \leqslant 0$ has been used, such that the functions $\Phi_i = \Phi_i[\overline{\mathbf{M}}, Q]$ play the role of *overstress functions*. From now on the case of *isotropy* is considered. Then the co-variant tensor $\overline{\mathbf{C}}_e$ and the contra-variant tensor $\partial \Psi / \partial \overline{\mathbf{C}}_e$ occurring in Eq. (8) commute such that, with $\overline{\mathbf{G}}^{\flat}$ introduced in Appendix A,

$$\overline{\mathbf{C}}_e \cdot \frac{\partial \Psi}{\partial \overline{\mathbf{C}}_e} \cdot \overline{\mathbf{G}}^{\flat} = \overline{\mathbf{G}}^{\flat} \cdot \frac{\partial \Psi}{\partial \overline{\mathbf{C}}_e} \cdot \overline{\mathbf{C}}_e = \left(\overline{\mathbf{C}}_e \cdot \frac{\partial \Psi}{\partial \overline{\mathbf{C}}_e} \cdot \overline{\mathbf{G}}^{\flat} \right)^t \tag{13}$$

The above relation can be verified by a spectral decomposition for $\overline{\mathbf{C}}_e$. Consequently, from Eq. (8.1) it follows that

$$\operatorname{sym}[\overline{\mathbf{M}} \cdot \overline{\mathbf{G}}^{\flat}] = \overline{\mathbf{M}} \cdot \overline{\mathbf{G}}^{\flat}, \quad \operatorname{skew}[\overline{\mathbf{M}} \cdot \overline{\mathbf{G}}^{\flat}] = \mathbf{0} \tag{14}$$

which reveals the co-variant representation of the Mandel stress tensor $\overline{\mathbf{M}} \cdot \overline{\mathbf{G}}^{\flat}$ as symmetric. Thus

$$\overline{\mathbf{G}}^{\flat} \cdot \frac{\partial \Phi_i^*}{\partial \overline{\mathbf{M}}} = \overline{\mathbf{G}}^{\flat} \cdot \frac{\partial \Phi_i^*}{\partial (\overline{\mathbf{M}} \cdot \overline{\mathbf{G}}^{\flat})} \cdot \overline{\mathbf{G}}^{\flat} = \left(\overline{\mathbf{G}}^{\flat} \cdot \frac{\partial \Phi_i^*}{\partial (\overline{\mathbf{M}} \cdot \overline{\mathbf{G}}^{\flat})} \cdot \overline{\mathbf{G}}^{\flat} \right)^t, \quad i = 1, \ldots, S \tag{15}$$

which implies for the flow rule (10)

$$\operatorname{sym}[\overline{\mathbf{G}}^{\flat} \cdot \overline{\mathbf{L}}_c] = \sum_{i=1}^{S} w_i \dot{\Lambda}_i \overline{\mathbf{G}}^{\flat} \cdot \frac{\partial \Phi_i^*}{\partial \overline{\mathbf{M}}}, \operatorname{skew}[\overline{\mathbf{G}}^{\flat} \cdot \overline{\mathbf{L}}_c] = \mathbf{0}. \tag{16}$$

The interpretation is, that for isotropy a non-associative concept based on a creep potential dependent on the Mandel stress tensor renders the flow rule in a co-variant formulation as a symmetric tensor.

As explained below alternative mixed-variant representations of the above flow rule (10) relative to the configurations $\overline{\mathscr{B}}, \mathscr{B}, \mathscr{B}_0$, are as follows:

$$\begin{aligned} &1.\ \overline{\mathscr{B}}: \overline{\mathbf{L}}_c = -\frac{1}{2} \mathscr{L}_c^{\sharp}[\overline{\mathbf{G}}^{\sharp}] \cdot \overline{\mathbf{G}}^{\flat} = \sum_{i=1}^{S} w_i[\overline{\mathbf{M}}] \dot{\Lambda}_i \frac{\partial \Phi_i^*}{\partial \overline{\mathbf{M}}}, \\ &2.\ \mathscr{B}: -\frac{1}{2} \mathscr{L}^{\sharp}[\mathbf{b}_e] \cdot \mathbf{b}_e^{-1} = \sum_{i=1}^{S} w_i[\mathbf{m}] \dot{\Lambda}_i \frac{\partial \Phi_i^*}{\partial \mathbf{m}}, \quad \text{where } \mathbf{m} = {}^*\Phi_e'(\overline{\mathbf{M}}) = \mathbf{F}_e^{-t} \cdot \overline{\mathbf{M}} \cdot \mathbf{F}_e^t \\ &3.\ \mathscr{B}_0: -\frac{1}{2} \partial_t \mathbf{C}_c^{-1} \cdot \mathbf{C}_c = \sum_{i=1}^{S} w_i[\mathbf{M}] \dot{\Lambda}_i \frac{\partial \Phi_i^*}{\partial \mathbf{M}}, \quad \text{where } \mathbf{M} = {}^*\Phi_c'(\overline{\mathbf{M}}) = \mathbf{F}_c^t \cdot \overline{\mathbf{M}} \cdot \mathbf{F}_c^{-t} \end{aligned} \tag{17}$$

The flow rule (17.1) is obtained by inserting $\overline{\mathbf{L}}_c = -1/2 \mathscr{L}_c^{\sharp}[\overline{\mathbf{G}}^{\sharp}] \cdot \overline{\mathbf{G}}^{\flat}$ into the relation (10). Here additionally the creep Lie derivative operator $\mathscr{L}_c^{\sharp}[\bullet] = {}_*\Phi_c^{\sharp}[\partial_t[{}^*\Phi_c^{\sharp}[\bullet]]]$ has been used, were ${}^*\Phi_c^{\sharp}$ is explained in Eq. (A.3.1) and ${}_*\Phi_c^{\sharp}$ denotes its inverse operation. An elastic push-forward ${}_*\Phi_e[\bullet]\mathbf{F}_e \cdot [\bullet] \cdot \mathbf{F}_e^{-1}$ of the flow rule (17.3) renders the relation (17.2). Here the mixed variant Kirchhoff stress tensor is obtained from $\mathbf{m} = {}_*\Phi_e'[\overline{\mathbf{M}}]$, and $\mathbf{b}_e$ is introduced in Eq. (A.3). Furthermore the Lie derivative operator $\mathscr{L}^{\sharp}[\bullet] = {}_*\Phi^{\sharp}[\partial_t[{}^*\Phi^{\sharp}[\bullet]]]$ has been used, were ${}^*\Phi^{\sharp}$ is explained in Eq. (A.3.1) and ${}_*\Phi^{\sharp}$ denotes its inverse operation. The flow rule (17.3) w.r.t. the reference configuration is a consequence of a creep pull-back ${}^*\Phi_c[\bullet] = \mathbf{F}_c^{-1} \cdot (\bullet) \cdot \mathbf{F}_c$ of the flow rule Eq. (17.1), where the notation $\partial_t(.)$ denotes the time derivative. Lastly we note the following restrictions for the weighting functions

$$w_i[\overline{\mathbf{M}}] = w_i[\mathbf{m}] = w_i[\mathbf{M}], \quad i = 1, \ldots, S. \tag{18}$$

3. Formulation of stress mode related weighting functions at large strains

The weighting functions w_i for the flow rule Eq. (17) are firstly introduced in Eq. (11) to be dependent on the Mandel stress tensor $\overline{\mathbf{M}}$, which is related to the intermediate configuration $\overline{\mathscr{B}}$. However, in order to associate the weighting functions to stress states which can be investigated experimentally in the laboratory, it is natural to consist stress modes relative to the actual configuration $\mathscr{B}$, where the Cauchy stress tensor $\boldsymbol{\sigma}$ defines the true stress state.

In the following we will concentrate on the two independent stress modes of tension and compression with applications to isotropic materials. In order to have a quantity which serves as an indicator for the related stress mode, we define the Lode angle (stress mode angle)

$$\begin{aligned} &1.\ \theta = \frac{1}{3}\arccos[\xi], \quad \text{where} \\ &2.\ \xi = \frac{\sqrt{27}}{2}\frac{{}^{\sigma_{\text{dev}}}I_3}{\left({}^{\sigma_{\text{dev}}}I_2\right)^{3/2}} \\ &3.\ {}^{\sigma_{\text{dev}}}I_i = \frac{1}{i}\mathbf{g}^{\flat} : (\boldsymbol{\sigma}_{\text{dev}})^i, \qquad i = 2,3. \end{aligned} \tag{19}$$

Upon using the definition (19.1), the weighting functions $w_i[\theta]$ for the loading of tension and compression ($S = 2$) can be rewritten in terms of the stress mode factor ξ as

$$\begin{aligned} &1.\ \text{tension} : w_1[\xi] = \frac{1}{2}(1+\xi) \\ &2.\ \text{compression} : w_2[\xi] = \frac{1}{2}(1-\xi). \end{aligned} \tag{20}$$

More details about the stress mode angle θ, the stress mode factor ξ and the weighting functions $w_i[\theta]$ have been introduced in Mahnken (2005b) and Shaban et al. (2007) which shall not be repeated here.

In order to verify the restriction (18) firstly we note the relations $\boldsymbol{\tau} = J\boldsymbol{\sigma}$ and $\mathbf{m} = \mathbf{g}^{\flat}\cdot\boldsymbol{\tau}$ for the Kirchhoff stress tensor and the mixed variant Kirchhoff stress tensor, respectively. It follows, that alternatively the stress mode angle Eq. (19) can be expressed as

$$\begin{aligned} &1.\ \theta = \frac{1}{3}\arccos[\xi], \quad \text{where} \\ &2.\ \xi = \frac{\sqrt{27}}{2}\frac{{}^{\tau'_{\text{dev}}}I_3}{\left({}^{\tau'_{\text{dev}}}I_2\right)^{3/2}} \\ &3.\ {}^{\tau'_{\text{dev}}}I_i = \frac{1}{i}\mathbf{1}^{\backprime} : (\mathbf{m}^{\text{dev}})^i, \qquad i = 2,3. \end{aligned} \tag{21}$$

Furthermore, upon exploiting the relations

$$\begin{aligned} &\overline{\mathbf{M}}^{\text{dev}} = {}^{*}\Phi'_e[\mathbf{m}^{\text{dev}}] \quad \Rightarrow {}^{\tau'_{\text{dev}}}I_i = {}^{\overline{T}_{\text{dev}}}I_i, \quad \text{where } {}^{\overline{T}_{\text{dev}}}I_i = \frac{1}{i}\overline{\mathbf{1}}^{\backprime} : (\overline{\mathbf{M}}^{\text{dev}})^i, \quad i = 2,3 \\ &\mathbf{M}^{\text{dev}} = {}^{*}\Phi'[\mathbf{m}^{\text{dev}}] \quad \Rightarrow {}^{\tau'_{\text{dev}}}I_i = {}^{T_{\text{dev}}}I_i, \quad \text{where } {}^{T_{\text{dev}}}I_i = \frac{1}{i}\mathbf{1}^{\backprime} : (\mathbf{M}^{\text{dev}})^i, \quad i = 2,3 \end{aligned} \tag{22}$$

finally ensures the relations (18).

4. Modelling of stress mode dependent thermoviscoplasticity at large strains

4.1. Prototype model

Upon applying the thermodynamic framework of the previous sections to a specific free energy function, an overstress function and a creep potential, respectively, the purpose of this subsection is the formulation of a constitutive equations capable to simulate the asymmetry in creep within a geometrically nonlinear theory, and, furthermore, to satisfy the thermodynamic restrictions. The constitutive relations formulated relative to the intermediate configuration $\overline{\mathscr{B}}$ in terms of contra-variant tensor objects are summarised in Eq. (I) to Eq. (X) of Table 1. The multiplicative decomposition of the deformation gradient is introduced in Eq. (I). The quantity e_v in Eq. (II) is a strain-like internal variable which describes the hardening state of the material with associated material parameters q, b and H. As a specific example of a free energy function we consider Eq. (III) in Table 1.

The free energy function Ψ is splitted into two parts (thermoelastic and inelastic) as introduced in Eq. (III.1). The thermoelastic part Ψ^{el} is given in Eq. (III.2). Therein, the first term represents the free energy due to volumetric deformations (cf. Simo and Pister, 1984) and the second term describes the energy storage as a result of isochoric thermoelastic strains (cf. Simo et al., 1985; Simo, 1988). The third term models the thermoelastic coupling phenomena. The last two terms of Eq. (III.2) describe the energy storage due to thermal effects. In the thermoelastic part of the free energy, $K[\vartheta]$ and $G[\vartheta]$ are the bulk modulus and the shear modulus respectively. Moreover, $\alpha[\vartheta]$ defines the coefficient of thermal expansion, ϑ_0 represents the reference temperature, c_d is the specific heat capacity. In addition to the thermoelastic part of the free energy, the inelastic part Ψ^p of the free energy is defined in Eq. (III.3) (cf. Lemaitre and Chaboche, 1990) in order to describe the energy storage due to viscoplastic deformations.

Table 1
Constitutive relations for stress mode dependent thermoviscoplasticity related to the intermediate configuration

I. Kinematic decomposition

$$\mathbf{F} = \mathbf{F}_e \cdot \mathbf{F}_c$$

II. Strain like internal variable

$$q = e_v$$

III. Free energy function

1. $\rho_R \Psi = \rho_R \Psi^{el}[\overline{\mathbf{C}}_e, \vartheta] + \rho_R \Psi^{p}[e_v, \vartheta]$, where
2. $\rho_R \Psi^{el} = \frac{1}{2} K[\vartheta](\ln J_e)^2 + \frac{G[\vartheta]}{4}(\mathrm{tr}(\ln \hat{\mathbf{C}}_e)^2) - 3K[\vartheta]\alpha[\vartheta](\vartheta - \vartheta_0)(\ln J_e) + c_d[\vartheta](\vartheta - \vartheta_0) - c_d[\vartheta]\vartheta \ln\left(\frac{\vartheta}{\vartheta_0}\right)$
3. $\rho_R \Psi^{p} = q\left(e_v + \frac{1}{b}\exp(-be_v)\right) - \frac{q}{b} + \frac{1}{2}He_v^2$

IV. Mandel stress tensor and stress-like internal variables

1. $\overline{\mathbf{M}} = 2\overline{\mathbf{C}}_e \cdot \rho_R \frac{\partial \Psi}{\partial \overline{\mathbf{C}}_e} = K[\vartheta]\ln J_e \mathbf{1} + G[\vartheta]\mathrm{dev}\ln \overline{\mathbf{C}}_e - 3K[\vartheta]\alpha[\vartheta](\vartheta - \vartheta_0)\mathbf{1}$
2. $R = \rho_R \frac{\partial \Psi}{\partial e_v} = q(1 - \exp(-be_v)) + He_v$

V. Overstress function and creep potential

$$\Phi[\hat{\overline{\mathbf{M}}}, R] = \Phi^*[\hat{\overline{\mathbf{M}}}, R] = \sigma_v - J(Y_0 + R), \quad \sigma_v = \sqrt{\frac{3}{2}}||\hat{\overline{\mathbf{M}}}^{\mathrm{dev}}|| = \sqrt{\frac{3}{2}}||\overline{\mathbf{M}}^{\mathrm{dev}}||$$

VI. Flow rule

1. $\overline{\mathbf{L}}_c = \dot{\Lambda}\overline{\mathbf{N}}$
2. $\dot{\Lambda} = \sum_{i=1}^{S} w_i \dot{\Lambda}_i$

VII. Flow factor associated to each mode

$$\dot{\Lambda}_i = A_i \exp\left(-\frac{\Delta U}{R_g \vartheta}\right)\left(\frac{\langle \Phi \rangle}{\sigma_0}\right)^{m_i} \quad i = 1, \ldots, S$$

VIII. Flow direction

$$\overline{\mathbf{N}} = \frac{\partial \Phi^*}{\partial \hat{\overline{\mathbf{M}}}} = \sqrt{\frac{3}{2}}\frac{(\overline{\mathbf{M}}^{\mathrm{dev}})^t}{||\overline{\mathbf{M}}^{\mathrm{dev}}||} = \sqrt{\frac{3}{2}}\frac{(\hat{\overline{\mathbf{M}}}^{\mathrm{dev}})^t}{||\hat{\overline{\mathbf{M}}}^{\mathrm{dev}}||}$$

IX. Equivalent inelastic strain

$$\dot{e}_v = J\dot{\Lambda}$$

X. Material parameters

$$\boldsymbol{\kappa} = [K, G, A_i, m_i, \{i = 1, \ldots, S\}, Y_0, q, b, H, \Delta U]^T$$

In Eq. (IV.1) the Mandel stress tensor $\overline{\mathbf{M}}$ is obtained from the relation (8.1) applied to the free energy function in Eq. (III). The first two terms in Eq. (IV.1) represent the spherical and deviatoric stress tensors whereas the third term represents the thermomechanical coupling. Next, we identify the stress-like and strain-like internal variables as $Q = [R]$ and $q = [e_v]$, respectively. Then the relation (8.2) yields the hardening variable R as the thermodynamic force conjugate to the internal variable e_v as summarised in Eq. (IV.2) of Table 1. The two terms of R represent a mixed nonlinear and linear isotropic hardening.

Concerning the creep potentials and the overstress functions introduced in Eq. (10) and Eq. (12) the following simplification is made

$$\Phi = \Phi_i = \Phi_i^* = \Phi^*, \quad i = 1, \ldots, S. \tag{23}$$

Furthermore, we restrict the dependency of these functions on the second invariant of the deviatoric effective Mandel stress tensor $\hat{\overline{\mathbf{M}}}$. This renders Eq. (V) in Table 1 for the overstress function $\Phi[\hat{\overline{\mathbf{M}}}^{\mathrm{dev}}, Q]$ and the creep potential $\Phi^*[\hat{\overline{\mathbf{M}}}^{\mathrm{dev}}, Q]$. Recall, that $J = \det[\mathbf{F}]$ is the determinant of the deformation gradient $\mathbf{F}$ introduced in Appendix A.

The general flow rule formulated for the creep velocity $\overline{\mathbf{L}}_c$ is obtained in Eq. (VI.1) of Table 1 by the application of Eq. (17.1) to the creep potential Φ^* of Eq. (V). Eq. (VI.2) in Table 1 represents the weighted decomposition of the flow factor $\dot{\Lambda}$ into individual flow factors $\dot{\Lambda}_i$. Based on a Norton structure of the relation (12.a) these are specified in Eq. (VII). Note, that the constants A_i and m_i are material parameters associated to the i-th mode where all the material parameters of the proposed model are summarized in Eq. (X). Furthermore, Eq. (VIII) specifies the flow direction $\overline{\mathbf{N}}$, which as a consequence of the relation (23), is identical for all stress modes. The evolution of the equivalent inelastic strain is given in Eq. (IX). Finally we note, that the notation $\langle \Phi \rangle = x$ for $x > 0$, $\langle \Phi \rangle = 0$ for $x \leqslant 0$ introduced in Table 1 renders the following relations for the flow factor

$$\dot{\Lambda}_i = 0 \quad \text{for} \quad \Phi \leqslant 0, \quad \dot{\Lambda}_i > 0 \quad \text{for} \quad \Phi > 0. \tag{24}$$

4.2. Thermodynamic consistency

According to the second law of thermodynamics the dissipation inequality (9) must be satisfied for the evolution equations. Using the expressions Eq. (VI.2) and Eq. (VIII) in Table 1 for the flow rule we obtain

$$\rho_R \mathscr{D}_{\mathrm{loc}}^{\mathrm{red}} = \overline{\mathbf{M}} : \overline{\mathbf{L}}_c - Q \frac{\partial q}{\partial t} = \overline{\mathbf{M}} : \overline{\mathbf{L}}_c - R\dot{e}_v = \overline{\mathbf{M}} : \dot{\Lambda} \sqrt{\frac{3}{2}} \frac{(\overline{\mathbf{M}}^{\mathrm{dev}})^t}{||\overline{\mathbf{M}}^{\mathrm{dev}}||} - JR\dot{\Lambda}, \tag{25}$$

and using Eq. (V) in Table 1, the reduced dissipation is written as

$$\rho_R \mathscr{D}_{\mathrm{loc}}^{\mathrm{red}} = \dot{\Lambda}(\sigma_v - JR) = \dot{\Lambda}(\Phi + JY_0). \tag{26}$$

Due to the relations (24) the reduced dissipation satisfies

$$\rho_R \mathscr{D}_{\mathrm{loc}}^{\mathrm{red}} \geqslant JY_0 \dot{\Lambda} \geqslant 0. \tag{27}$$

5. Numerical implementation at large strains

In this section the numerical integration of the evolution equations of the previous sections is briefly described. To this end we consider a finite time step $\Delta t = {}^{n+1}t - {}^{n}t$ with given initial data ${}^{n}e_v, {}^{n}\mathbf{C}_c^{-1} = {}^{n}\mathbf{F}^{-1} \cdot {}^{n}\mathbf{b}_e \cdot {}^{n}\mathbf{F}^{-t}$, deformation gradient ${}^{n+1}\mathbf{F}$ and its determinant ${}^{n+1}J = \det[{}^{n+1}\mathbf{F}]$. For our purpose an exponential map integrator is applied to the flow rule (17.3) (see e.g. Eterovic and Bathe (1990) and Simo (1992)).

5.1. Integration scheme

An Euler backward rule is applied to the rate equations (VI.1) and (VI.2) of Table 1. By the use of Eq. (IX), this leads to the following incremental objective integration algorithm with respect to the actual configuration (compare also the similar approach described in Steinmann et al., 1993 and Mahnken, 2000).

$$\begin{aligned} &1.\ {}^{n+1}\mathbf{b}_e = \exp(-2\,\Delta\Lambda\, {}^{n+1}\mathbf{n}) \cdot {}^{n+1}\mathbf{b}^{\mathrm{tr}}, \quad \text{where } {}^{n+1}\mathbf{b}^{\mathrm{tr}} = {}^{n+1}\mathbf{F} \cdot {}^{n}\mathbf{C}_c^{-1} \cdot {}^{n+1}\mathbf{F}^T \\ &2.\ {}^{n+1}e_v = {}^{n}e_v + \Delta e_v. \end{aligned} \tag{28}$$

Here the increments on the r.h.s in the above equations are obtained from

$$\begin{aligned} &1.\ \Delta\Lambda = \sum_{i=1}^{S} \Delta\Lambda_i w_i \\ &2.\ \Delta\Lambda_i = \Delta t A_i \exp\left(-\frac{\Delta U}{R_g \vartheta}\right) \left(\frac{\langle \Phi \rangle}{\sigma_0}\right)^{m_i} \\ &3.\ w_i = w_i[\xi] (\text{see Eq. (20)}) \\ &4.\ \sigma_v^2 = \frac{3}{2} \hat{\boldsymbol{\tau}}^{\mathrm{dev}} : \hat{\boldsymbol{\tau}}^{\mathrm{dev}} = 3^{\tau'_{\mathrm{dev}}} I_2 \\ &5.\ \mathbf{n} = \frac{3}{2\sigma_v} \hat{\boldsymbol{\tau}}^{\mathrm{dev}} \\ &6.\ R = q(1 - \exp(-be_v)) + He_v \\ &7.\ \Phi = \sigma_v - J(Y_0 + R) \\ &8.\ \Delta e = J\Delta\Lambda, \end{aligned} \tag{29}$$

where for notational brevity the index $n+1$ referring to the actual time step has been neglected. Without going into detail we follow the derivations of Simo (1992) thus rendering the Kirchhoff stresses as

$$\begin{aligned}
&\boldsymbol{\tau} = \hat{\boldsymbol{\tau}}^{\mathrm{vol}} + \hat{\boldsymbol{\tau}}^{\mathrm{dev}} \quad \text{and} \\
&\hat{\boldsymbol{\tau}}^{\mathrm{vol}} = p\mathbf{g}^{\sharp}, \quad p = K(\ln J^{\mathrm{tr}} - 3\alpha(\vartheta - \vartheta_0)), \quad J^{\mathrm{tr}} = \det[\mathbf{b}^{\mathrm{tr}}]^{1/2} \\
&\hat{\boldsymbol{\tau}}^{\mathrm{dev}} = \hat{\boldsymbol{\tau}}^{\mathrm{dev,tr}} - 2G\Delta\Lambda\mathbf{n}, \quad \text{where} \quad \hat{\boldsymbol{\tau}}^{\mathrm{dev,tr}} = G\,\mathrm{dev}\ln\mathbf{b}^{\mathrm{tr}}.
\end{aligned} \tag{30}$$

Upon using a spectral decomposition of the right elastic Cauchy Green tensor and using the fact, that due to isotropy $\mathbf{b}^{\mathrm{tr}}$ and $\boldsymbol{\tau}$ commute, we have

$$1.\ \mathbf{b}^{\mathrm{tr}} = \sum_{A=1}^{3} (\lambda_A^{\mathrm{tr}})^2 \mathbf{m}_A \Rightarrow \quad 2.\ \hat{\boldsymbol{\tau}} = \sum_{A=1}^{3} \beta_A \mathbf{m}_A. \tag{31}$$

Here $\beta_A, A = 1,2,3$ are the principal values of the effective Kirchhoff stresses, which by use of the vector/matrix notations

$$\underline{\varepsilon}^{\mathrm{tr}} := \begin{bmatrix} \ln\lambda_1^{\mathrm{tr}} \\ \ln\lambda_2^{\mathrm{tr}} \\ \ln\lambda_3^{\mathrm{tr}} \end{bmatrix}, \quad \underline{\beta} := \begin{bmatrix} \beta_1 \\ \beta_2 \\ \beta_3 \end{bmatrix}, \quad \underline{1} := \begin{bmatrix} 1 \\ 1 \\ 1 \end{bmatrix}, \quad \underline{I}_3 := \begin{bmatrix} 1 & & \\ & 1 & \\ & & 1 \end{bmatrix}, \quad \underline{I}_3^{\mathrm{dev}} := \underline{I}_3 - \frac{1}{3}\underline{1}\otimes\underline{1} \tag{32}$$

satisfy

$$\begin{aligned}
&\underline{\beta} = \hat{\underline{\beta}}^{\mathrm{vol}} + \hat{\underline{\beta}}^{\mathrm{dev}} \quad \text{and} \\
&\hat{\underline{\beta}}^{\mathrm{vol}} = p\underline{1}, \quad p = K(\underline{1}\cdot\underline{\varepsilon}^{\mathrm{tr}} - 3\alpha(\vartheta - \vartheta_0)) \\
&\hat{\underline{\beta}}^{\mathrm{dev}} = \hat{\underline{\beta}}^{\mathrm{dev,tr}} - 2G\Delta\lambda\underline{y}, \quad \text{where} \quad \hat{\underline{\beta}}^{\mathrm{dev,tr}} = 2G\underline{I}_3^{\mathrm{dev}}\cdot\underline{\varepsilon}^{\mathrm{tr}}, \quad \underline{y} = \frac{\hat{\underline{\beta}}^{\mathrm{dev}}}{\sqrt{\frac{3}{2}}\|\hat{\underline{\beta}}^{\mathrm{dev}}\|}.
\end{aligned} \tag{33}$$

Note that $\underline{I}_3^{\mathrm{dev}}$ is defined as $\underline{I}_3^{\mathrm{dev}}\cdot\underline{a} = \underline{a}^{\mathrm{dev}}$ where $\mathrm{tr}(\underline{a}^{\mathrm{dev}}) = 0$ and $\underline{a} \in IR^3$. The previous sets of Eqs. (32) and (33) can be regarded as the counterpart of the relations (30) in the principal directions. Note, that the above structure for the principal Kirchhoff stresses is identical as in the geometrically linear theory. This allows the algorithm developed in Shaban et al. (2007) where the resulting set of algebraic equations is reduced to one single scalar equation dependent on one unknown $\Delta\Lambda$.

5.2. Algorithmic tangent modulus

The finite element equilibrium iteration requires the spatial algorithmic tangent operator defined as $\mathbb{c} = 2\partial\boldsymbol{\tau}/\partial\mathbf{g}^{\flat}$. As shown in Simo (1992) and Mahnken (1999) the result is

$$\mathbb{c} = \sum_{A=1}^{3}\sum_{B=1}^{3} \frac{\mathrm{d}\beta_A}{\mathrm{d}\varepsilon_B^{\mathrm{tr}}} \mathbf{m}_A\otimes\mathbf{m}_B + \sum_{A=1}^{3} 2\beta_A \frac{\mathrm{d}\mathbf{m}_A}{\mathrm{d}\mathbf{g}^{\flat}} + \sum_{A=1}^{3} J\frac{\mathrm{d}\beta_A}{\mathrm{d}J}\mathbf{m}_A\otimes\mathbf{g}^{\sharp} \tag{34}$$

where the detailed expression for $\mathrm{d}\mathbf{m}_A/\mathrm{d}\mathbf{g}^{\flat}$ is given in Simo (1992). As remarked in Simo (1992) the above result incorporates also $\mathrm{d}\beta_A/\mathrm{d}\varepsilon_B^{\mathrm{tr}}$, which is the consistent tangent operator of the geometrically linear theory, and which for the case with asymmetric effects has been developed in Shaban et al. (2007).

6. Simulation of laser transmission welding

6.1. Principle and modelling of laser transmission welding

The proposed constitutive model is used to simulate the laser transmission welding (LTW) process. In the LTW a laser-transparent and a laser-absorbent semi-finished product are joined together, thus ensuring that the adherends come into contact with each other (see Fig. 1).

The laser beam passes through the transparent part virtually unimpeded and is converted into heat as it is absorbed by the absorbent semi-finished product. The adherend that is transparent to the laser beam heats up through thermal conduction, therefore the adherends weld together. The reader is referred to Potente et al. (2006), Shaban et al. (2007) and Potente et al. (2008) for a detailed description of the LTW process.

Our concern is devoted to the simulation of contour LTW, which is one type of the LTW processes. In this process, the laser beam is moved along the weld with relatively slow speeds (V = 0.1–500 mm/s). The weld is only heated up on a partial basis, i.e. only part of the weld is melted, and there is no melting displacement.

A simulation of the contour LTW process is performed with the finite element program (ABAQUS-Version 6.5, 2004) using the two dimensational discretization of Fig. 2. The transparent part is shown in the left of Fig. 2, while the absorbant part is shown in the right. The joining surface coincides with the vertical centerline. The total length of the two parts is 12 mm while the width is 1.35 mm. The mesh for the LTW process in Fig. 2 consists of elements with 8-node biquadratic displacements, bilinear temperature and reduced integration with linear pressure. The mesh has 105×17 elements, which means that the number of elements is 1785 and the number of nodes is 5600.

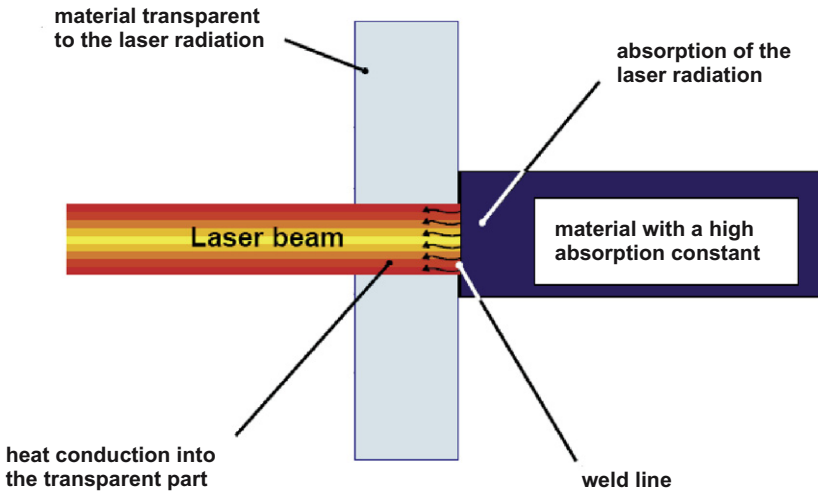

Fig. 1. Principle of the laser transmission welding process (Potente et al., 2002).

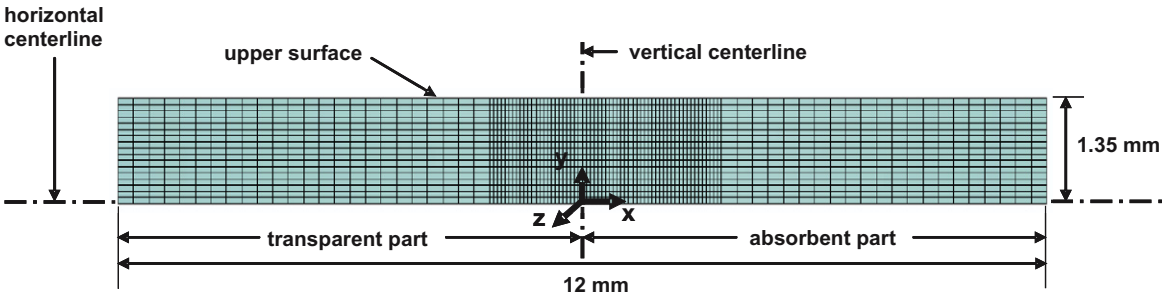

Fig. 2. The finite element mesh of the laser transmission welding process.

The lower surface is chosen as a symmetry boundary about the x-axis while the left and the right surfaces are constrained in the x-direction. The thermal effects of the convection and radiation in the upper surface are taken into account. The laser power is treated as a body heat flux with a Gaussian distribution for its intensity. The scanning velocity of the laser beam is 30 mm/s.

6.2. Experimental data bases and parameter identification

The constitutive equations of Table 1 have been implemented into UMAT subroutine. The material of the simulated specimen is polycarbonate (Lexan 104 R, GE Plastics). Experimental results in Shaban et al. (2007) are recalled in Fig. 3. This figure presents the results of both, the uniaxial tensile and compression true stress - true strain curves of polycarbonate at two different strain rates (8.3×10^{-3} s^{-1} and 8.3×10^{-2} s^{-1}) and at three different temperatures (23, 70 and 120 °C). In total the number of experiments is 12. Note that for each experiment in tension and compression a newly prepared specimen has been used. It is observed that the yield stress increases with increasing strain rate. A similar increase of the yield stress is seen at lower temperatures. Furthermore the yield stress in compression is higher than that in tension for the same strain rate and temperature, thus revealing the asymmetric behaviour.

In Shaban et al. (2007) the corresponding material parameters have been obtained with the least squares method and are repeated in Table 2 of this work. The comparison of the experimental data with the simulated data is depicted in Fig. 3, and clearly demonstrates the capability of the constitutive equations to simulate the asymmetric behaviour of the material w.r.t. tension and compression.

The glass transition range of the polycarbonate is assumed to be between 140 °C and 150 °C. The effect of the temperature on Young's modulus is taken into account as mentioned in Shaban et al. (2007) using the following equation:

$$E[\vartheta] = \begin{cases} 1831.926 \quad \text{MPa}, & \text{if} \quad \vartheta \leqslant 140\,^{\circ}C \\ -183.56 \times \vartheta + 27536.0, & \text{if} \quad 140\,^{\circ}C < \vartheta \leqslant 150\,^{\circ}C \\ 2.0 \quad \text{MPa}, & \text{if} \quad \vartheta > 150\,^{\circ}C. \end{cases} \tag{35}$$

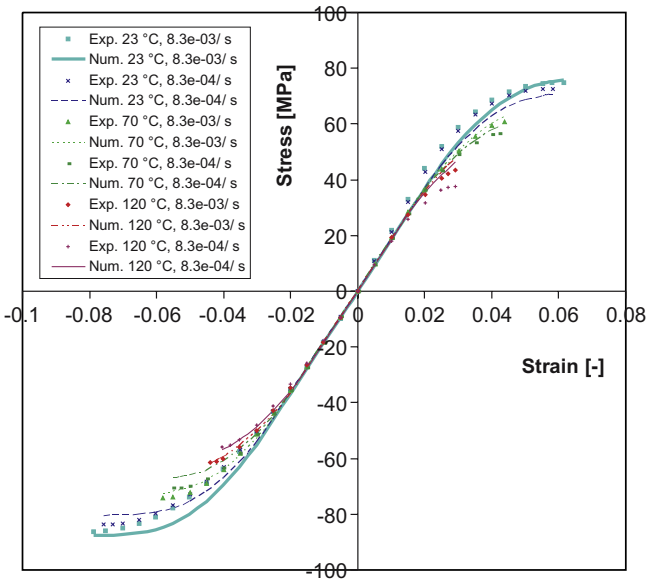

Fig. 3. Comparison between experimental and numerical data of the polycarbonate.

Table 2
Material parameters for polycarbonate corresponding to tension and compression modes

E [MPa]	ν [−]	Y_0 [MPa]	σ_0 [MPa]	b [−]	q [MPa]	H [MPa]
1831.926	0.38	5.718	10.0	236.297	21.689	43.636
A_1 [−]	m_1 [−]	A_2 [−]	m_2 [−]	R_g [J/mol K]	ΔU[J/mol]	
0.00589	21.45	0.0727	17.751	8.314	82.063×10^3	

The thermodynamic parameters of state such as the density ρ_R in Eq. (4), the specific heat capacity c_d in Eq. (III.2) of Table 1, the heat conductivity λ in Eq. (6) as well as the coefficient of thermal expansion α in Eq. (III.2) of Table 1 was implemented as temperature dependent properties as shown in Fig. 4.

6.3. Results and discussion

6.3.1. Temperature distribution

Fig. 5 shows the temperature development with time at three different positions in the horizontal centerline of Fig. 2, namely $x = 0.0$, 0.15 and 0.30 mm where x represents the x coordinate in Fig. 2. It can be seen that the temperature undergoes a pronounced increase during the time at which the laser acts, passing through the material's glass transition temperature. The temperature reaches its maximum value after about 0.3 s. After the laser has run through the welded parts, the material cools down slowly, passing through the glass transition temperature for a second time and then cools down to room temperature as shown in Fig. 5. In other words, the heating phase lasts about 0.3 s after which the cooling phase starts and continues. It is observed from Fig. 5 that the maximum temperature (291.1 °C) is found at a distance of 0.15 mm from the vertical centerline (the temperature at $x = 0$ mm is 224.5 °C and at $x = 0.30$ mm is 246.1 °C). This observation means that the maximum temperature is not located in the joining area but in the absorbing adherend behind.

6.3.2. Residual stresses

The residual Cauchy stresses are calculated using the proposed constitutive model at large strains. The residual stresses are observed at the point $x = 0.15$ mm, $y = 0.0$ mm (maximum stress), where x and y represent the x and y coordinates in Fig. 2 respectively. Compressive stresses are first seen to develop as a result of the thermal expansion (see Fig. 6). Following that, they drop to a very low level (zero value) when the glass transition temperature is reached. This abrupt change in the stress distribution happens during the glass transition range. The zero stress value is maintained for such a time in which the joining zone is in the molten state. During the cooling phase, tensile stresses develop after about 1.0 s, which increase to a maximum value and then relax as the cooling time increases.

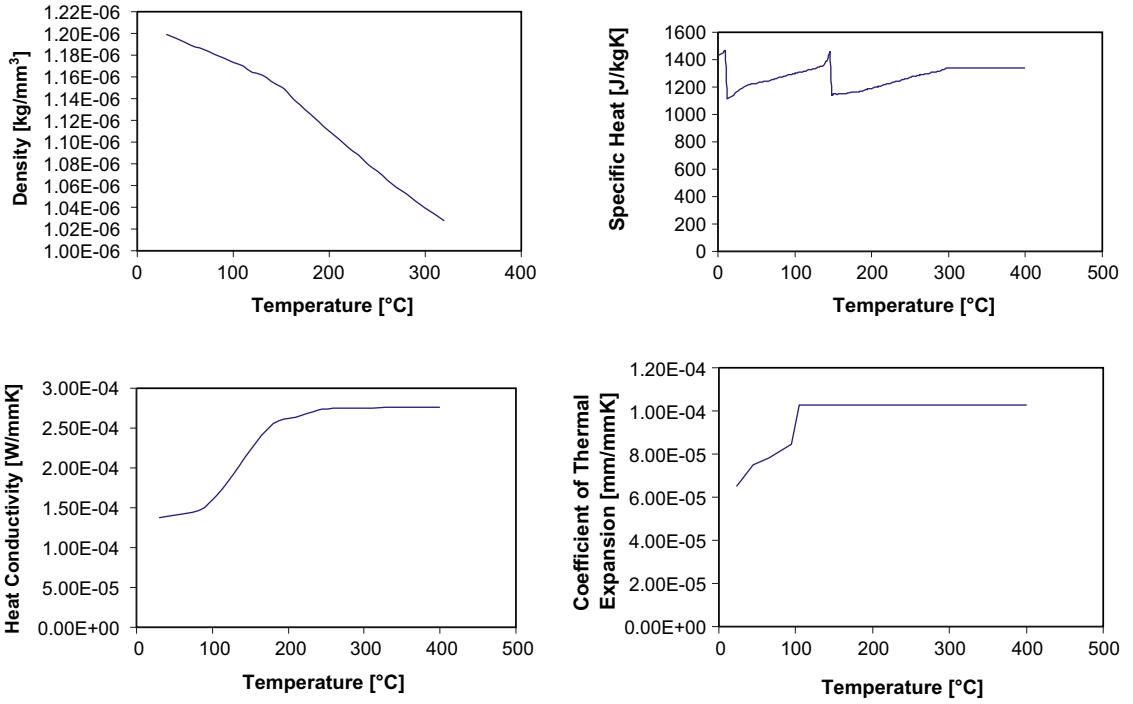

Fig. 4. Temperature dependency of experimental properties of polycarbonate: (top left) density and (top right) specific heat; (bottom left) heat conductivity and (bottom right) coefficient of thermal expansion.

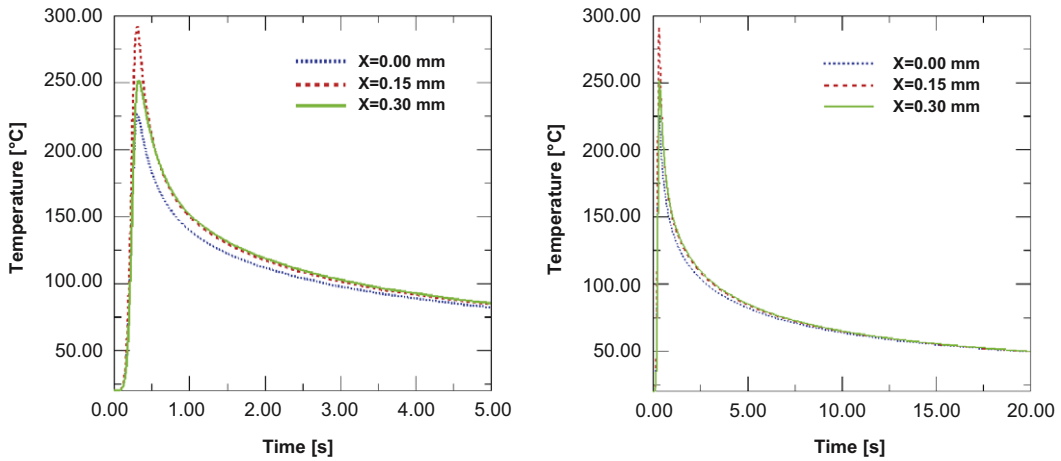

Fig. 5. Temperature distribution versus time at three different positions on the horizontal centerline of Fig. 2. The time is up to 5 s (left) and up to 20 s (right).

Comparing the stress components in different directions according to x,y and z coordinates of Fig. 2, it is seen in Fig. 6, that the stress component in z-direction has the highest stress value. In other words, in contour laser transmission welding, the maximum stresses occur in the direction of the part's length.

Fig. 7 detects the distribution of the stress component in z-direction at two different surfaces, namely the horizontal centerline and the upper surface of Fig. 2, after 20.0 s. The maximum stress is found in the absorbing material at the same position of the maximum temperature (x = 0.15 mm). While tensile stresses prevails in the region of the weld seam, compressive stresses are found in the neighbour material. It is observed that the stress peak values are higher in the centerline because it receives more heating energy than the upper surface. Furthermore it is clearly observed that the compressive and tensile stresses are not symmetric in magnitude which highlights the capability of the model equations to simulate the asymmetric effects.

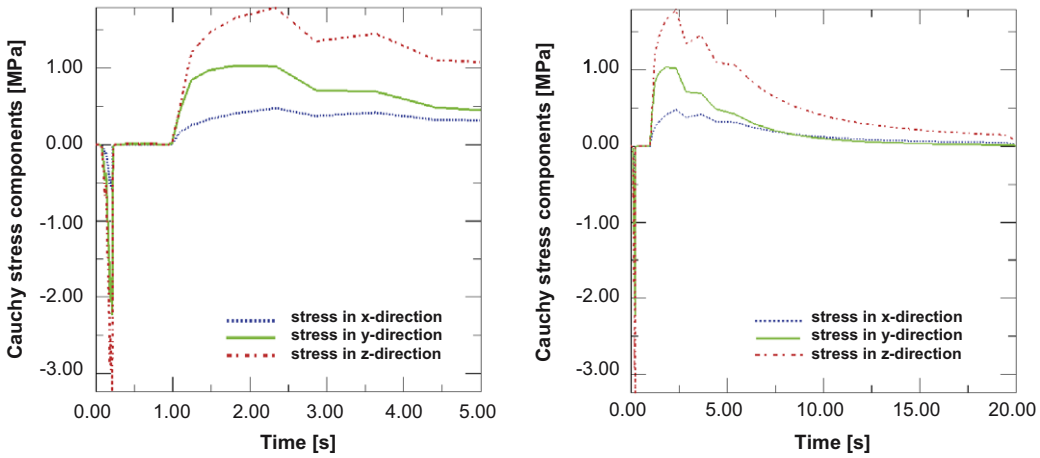

Fig. 6. Distribution of different Cauchy stress components versus time at $x = 0.15$ mm in the horizontal centerline of Fig. 2. The time is up to 5 s (left) and up to 20 s (right).

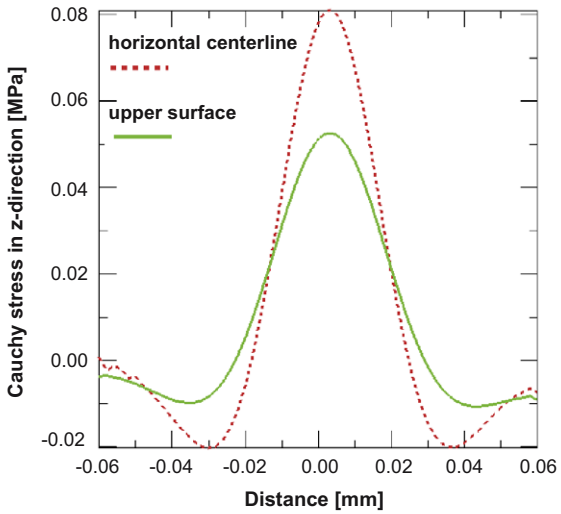

Fig. 7. Distribution of the Cauchy stress in z-direction along the horizontal centerline and the upper surface of Fig. 2.

7. Summary and conclusions

This contribution was directed to the simulation of asymmetric effects within a geometrically nonlinear theory. To this end a flow rule is postulated on the basis of a thermodynamic consistent framework in a mixed variant formulation. The flow rule is decomposed into a sum of weighted quantities, each of them related to a certain stress mode. The characterisation of the stress modes is obtained in the octahedral plane of the deviatoric stress space in terms of a single scalar variable, which enables for construction of scalar weighting functions. A main advantage of the concept is that the stress modes can directly be associated to certain characteristic loading scenarios, such as tension and compression, which are experimentally investigated in the laboratory.

Furthermore the numerical implementation of the model equations is described briefly, which has been implemented into the UMAT subroutine of the commercial finite element program ABAQUS. The simulation of the laser transmission welding process highlights the capability of the model equations to simulate the asymmetric effects for polycarbonate.

It appears, that the proposed model equations offer further flexibility to simulate asymmetric effects combined to different effects. Therefore the combination of asymmetry and induced anisotropy should constitute an area of the future research work.

Acknowledgments

This research was supported by the Deutsche Forschungsgemeinschaft (DFG) under grant Ma 1979/7-2. All experiments on polycarbonate specimens have been performed at the Institute of Plastics, University of Paderborn, Germany.

Appendix A. Basic concepts of tensor calculus on manifolds with application to multiplicative plasticity

A.1. Metric tensors and tensor invariants

Upon introducing an intermediate configuration $\overline{\mathscr{B}}$ in addition to a reference configuration $\mathscr{B}_0$ and a spatial configuration $\mathscr{B}$, the underlying concept of multiplicative elasto-plasticity assumes the decomposition of the deformation gradient $\mathbf{F}$ into elastic and creep parts, respectively, i.e.

$$\mathbf{F} = \mathbf{F}_e \cdot \mathbf{F}_c \tag{A.1}$$

The three associated tangent spaces $T\mathscr{B}_0, T\mathscr{B}$ and $T\overline{\mathscr{B}}$ are equipped with co-variant Riemannian metric tensors $\mathbf{G}^\flat, \mathbf{g}^\flat, \overline{\mathbf{G}}^\flat$, respectively, and analogously the associated dual spaces $T\mathscr{B}_0^*, T\mathscr{B}^*$ and $T\overline{\mathscr{B}}^*$ with contra-variant Riemannian metric tensors $\mathbf{G}^\sharp = (\mathbf{G}^\flat)^{-1}, \mathbf{g}^\sharp = (\mathbf{g}^\flat)^{-1}, \overline{\mathbf{G}}^\sharp = (\overline{\mathbf{G}}^\flat)^{-1}$, respectively, see e.g. Marsden and Hughes (1993), van der Giessen and Kollmann (1996) and Hackenberg (1992). The above tensor objects can be used to define invariants of second order tensors. E.g. we define all three *basic invariants* of a mixed-variant second order tensor $\overline{\mathbf{A}}' = \overline{A}_i^j \overline{\mathbf{G}}^i \otimes \overline{\mathbf{G}}_j$, related to the intermediate configuration as follows:

$${}^{\overline{A}'}I_i := \frac{1}{i}\overline{\mathbf{1}} : (\overline{\mathbf{A}}')^i = \frac{1}{i}\overline{\mathbf{1}}' : (\overline{\mathbf{A}})^i = \frac{1}{i}\overline{\mathbf{G}}^\sharp : (\overline{\mathbf{A}}' \cdot \overline{\mathbf{G}}^\flat)^i = \frac{1}{i}\overline{\mathbf{G}}^\flat : (\overline{\mathbf{A}} \cdot \overline{\mathbf{G}}^\sharp)^i, \quad i = 1,2,3. \tag{A.2}$$

Here $\overline{\mathbf{A}} = (\overline{\mathbf{A}}')^t$ and $\overline{\mathbf{1}} = \overline{\mathbf{G}}_i \otimes \overline{\mathbf{G}}^i = (\overline{\mathbf{1}}')^t$ is a (mixed-variant) second order unit tensor with basis vectors $\overline{\mathbf{G}}_i$ and $\overline{\mathbf{G}}^i$. In this respect the first and second relation of Eq. (A.2) represent the invariants as dual pairings of mixed-variant tensors. By use of $\overline{\mathbf{1}} = \overline{\mathbf{G}}^\flat \cdot \overline{\mathbf{G}}^\sharp$ these can also be written as dual pairings of co-variant and contra-variant tensors introduced in the third and fourth relation of Eq. (A.2). Without going into details we remark that in complete analogy to the relations (A.2) invariants can be defined relative to the reference configuration and the spatial configuration, respectively. To this end the (mixed-variant) second order unit tensors $\mathbf{1} = \mathbf{G}_i \otimes \mathbf{G}^i = (\mathbf{1}')^t$ and $\mathbf{1} = \mathbf{g}_i \otimes \mathbf{g}^i = (\mathbf{1})^t$, respectively, are introduced.

A.2. Strain tensors

Several strain measures can be constructed within the framework of multiplicative plasticity, see e.g. Haupt (2000), Marsden and Hughes (1993). In this work specific attention is directed to the following quantities:

$$\begin{aligned} &1.\ \mathbf{C}_c^{-1} := {}^*\Phi_c^\sharp[\overline{\mathbf{G}}^\sharp] = \mathbf{F}_c^{-1} \cdot \overline{\mathbf{G}}^\sharp \cdot \mathbf{F}_c^{-t} = \mathbf{F}^{-1} \cdot \mathbf{b}_e \cdot \mathbf{F}^{-t} = {}^*\Phi^\sharp[\mathbf{b}_e] \\ &2.\ \mathbf{b}_e := {}_*\Phi_e^\sharp[\overline{\mathbf{G}}^\sharp] = \mathbf{F}_e \cdot \overline{\mathbf{G}}^\sharp \cdot \mathbf{F}_e^t = \mathbf{F} \cdot \mathbf{C}_c^{-1} \cdot \mathbf{F}^t = {}_*\Phi^\sharp[\mathbf{C}_c^{-1}] \end{aligned} \tag{A.3}$$

Here the operators ${}^*\Phi_c^\sharp, {}^*\Phi_{,*}^\sharp \Phi_e^\sharp, {}_*\Phi^\sharp$ denote *creep pull-back*, *full pull-back*, *elastic push-forward*, and *full push-forward* operations of contra-variant tensor objects, respectively. An extended survey is given e.g. in Mahnken (2005a). Furthermore, in Eq. (A.3.1) $\mathbf{C}_c^{-1}$ is the inverse creep right Cauchy–Green tensor and $\mathbf{b}_e$ is the elastic left Cauchy–Green tensor. Upon replacing the contra-variant metric tensor $\overline{\mathbf{G}}^\sharp$ by the co-variant right elastic Cauchy–Green strain tensor $\overline{\mathbf{C}}_e = \mathbf{F}_e^t \cdot \mathbf{g}^\flat \cdot \mathbf{F}_e$, the relations (A.3) are written analogously as

$$\begin{aligned} &1.\ \mathbf{C} := {}^*\Phi_c^\flat[\overline{\mathbf{C}}_e] = \mathbf{F}_c^t \cdot \overline{\mathbf{C}}_e \cdot \mathbf{F}_c = \mathbf{F}^t \cdot \mathbf{g}^\sharp \cdot \mathbf{F} = {}^*\Phi^\flat[\mathbf{g}^\sharp] \\ &2.\ \mathbf{g}^\flat := {}_*\Phi_e^\flat[\overline{\mathbf{C}}_e] = \mathbf{F}_e \cdot \overline{\mathbf{G}}^\sharp \cdot \mathbf{F}_e^t = \mathbf{F} \cdot \mathbf{C} \cdot \mathbf{F}^t = {}_*\Phi^\flat[\mathbf{C}] \end{aligned} \tag{A.4}$$

Here the operators ${}^*\Phi_c^\flat, {}^*\Phi_{,*}^\flat \Phi_e^\flat, {}_*\Phi^\flat$ represent *creep pull-back*, *full pull-back*, *elastic push-forward* and *full push-forward* operations of co-variant tensor objects, respectively. Note, that $\mathbf{C}_c^{-1}$ is related to the reference configuration whereas $\overline{\mathbf{C}}_e$ is related to the intermediate configuration. Next, associated to $\overline{\mathbf{C}}_e$ and $\mathbf{b}_e$ the multiplicative splits

$$\mathbf{b}_e = J_e^{2/3}\hat{\mathbf{b}}_e, \overline{\mathbf{C}}_e = J_e^{2/3}\hat{\mathbf{C}}_e, \quad \text{where} \quad J_e = (\det[\overline{\mathbf{C}}_e \cdot \overline{\mathbf{G}}^\sharp])^{1/2} = (\det[\mathbf{g}^\sharp \cdot \mathbf{b}_e])^{1/2} \tag{A.5}$$

are introduced, such that $\hat{\mathbf{C}}_e, \hat{\mathbf{b}}_e$ and J_e represent the isochoric and volumetric part of the elastic deformation, respectively. Note, that the metric tensors $\overline{\mathbf{G}}^\sharp$ and $\mathbf{g}^\sharp$ are introduced in the above definitions for the determinants, thus allowing directly for unambiguous transformation between different configurations.

A.3. Rate of deformation tensors

Analogously to strain measures several rate of deformation tensors are defined in the literature, see e.g. Haupt (2000), Marsden and Hughes (1993). A well known quantity is the velocity gradient and its symmetric part

$$1.\ \mathbf{l} = \mathrm{grad}\mathbf{v} = \dot{\mathbf{F}} \cdot \mathbf{F}^{-1}, \quad 2.\ \mathbf{d} = \mathrm{sym}[\mathbf{g}^\flat \cdot \mathbf{l}] \tag{A.6}$$

where the time derivative of the displacement $\mathbf{u}$ defines the velocity $\mathbf{v} = \partial_t \mathbf{u}$. Note that $\mathbf{l} = l_j^i \mathbf{g}_i \otimes \mathbf{g}^j$ is a mixed variant tensor, which induces the symmetric rate of deformation tensor $\mathbf{d}$. An elastic pull-back renders the following quantities related to the intermediate configuration

$$\overline{\mathbf{L}} = {}^*\Phi_e^\flat[\mathbf{l}] = \mathbf{F}_e^{-1} \cdot \mathbf{l} \cdot \mathbf{F}_e \Rightarrow \overline{\mathbf{D}} = {}^*\Phi_e^\sharp[\mathbf{d}] = \mathbf{F}_e^t \cdot \mathbf{d} \cdot \mathbf{F}_e = \mathrm{sym}[\overline{\mathbf{C}}_e \cdot \overline{\mathbf{L}}]. \tag{A.7}$$

By use of the multiplicative decomposition (A.1) $\bar{\mathbf{L}}$ rewrites as

$$\bar{\mathbf{L}} := \bar{\mathbf{L}}_e + \bar{\mathbf{L}}_c, \quad \bar{\mathbf{L}}_e := \mathbf{F}_e^{-1} \cdot \dot{\mathbf{F}}_e, \quad \bar{\mathbf{L}}_c := \dot{\mathbf{F}}_c \cdot \mathbf{F}_c^{-1} = -\mathbf{F}_c \cdot \dot{\mathbf{F}}_c^{-1}, \tag{A.8}$$

such that $\bar{\mathbf{L}}_e$ and $\bar{\mathbf{L}}_c$ represent the elastic and creep parts, respectively, of the velocity gradient with respect to the intermediate configuration.

References

ABAQUS-Version 6.5, Users Manual, Hibbett, Karlsson & Sorensen, Inc., 2004.

Altenbach, H., Altenbach, J., Zolochevsky, A., 1995. Erweiterte Deformationsmodelle und Versagenskriterien der Werkstoffmechanik. Deutscher Verlag für Grundstoffindustrie, Stuttgart.

Arruda, E.M., Boyce, M.C., Jayachandran, R., 1995. Effects of strain rate, temperature and thermomechanical coupling on the finite strain deformation of glassy polymers. Mech. Mater. 19, 193–212.

Bertram, A., 2005. Elasticity and Plasticity of Large Deformations. Springer-Verlag, Berlin/Heidelberg/New York.

Betten, J., 1982a. Pressure-dependent yield behaviour of isotropic and anisotropic materials. In: P. Vermeer and H. Luger (Eds.), Deformation and Failure of Granular Materials, A.A. Balkema, Rotterdam, Presented at the IUTAM Symposium in Delft, September 1982, pp. 81–89.

Betten, J., 1982b. Net-stress analysis in creep mechanics. Ingenieur-Archiv 52, 405–419.

Betten, J., 1985. The classical plastic potential theory in comparison with the tensor function theory. Eng. Fract. Mechs. 21 (4), 641–652.

Betten, J., 2001. Mathematical modelling of materials behavior under creep conditions. Appl. Mech. Rev. 54 (2), 107–132.

Betten, J., 2004. Creep Mechanics, 2nd ed. Springer-Verlag, Berlin.

Betten, J., Borrmann, M., 1984. Einfluss der plastischen Kompressibitität und des Strength-Differential-Effektes auf das Fließerhalten von Sinter-und Polymerwerkstoffen. Rheologica Acta 23, 109–116.

Betten, J., Borrmann, M., 1987. Stationäres Kriechverhalten innendruckbelasteter dünnwandiger Kreiszylinderschalen unter Berücksichtigung des orthotropen Werkstoffverhaltens und des CSD-Effektes. Forschung im Ingenieurwesen 53 (3), 75–82.

Betten, J., Frosch, H.-G., Borrmann, M., 1982. Pressure-dependent yield behaviour of metals and polymers. Mater. Sci. Eng. 56, 233–246.

Boyce, M.C., Parks, D.M., Argon, A.S., 1988. Large inelastic deformation of glassy polymers, Part I: Rate dependent constitutive model. Mech. Mater. 7, 15–33.

Eterovic, A.L., Bathe, K.J., 1990. A hyperelastic based large strain elasto-plastic constitutive formulation with combined isotropic-kinematic hardening using the logarithmic stress and strain measures. Int. J. Num. Meth. Eng. 30, 1099–1114.

van der Giessen, E., Kollmann, F.G., 1996. On mathematical aspects of dual variables in continuum mechanics. Part 1: mathematical principles. ZAMM 76 (8), 447–462.

Hackenberg, H.P., 1992. Über die Anwendung inelastischer Stoffgesetze auf finite Deformationen mit der Methode der Finiten Elemente. Ph.D. Thesis, TH-Darmstadt.

Haupt, P., 2000. Continuum Mechanics and Theory of Materials. Springer-Verlag, Berlin.

Haward, R.N., Murphy, B.M., White, E.F.T., 1971. Relationship between compressive yield and tensile behavior in glassy thermoplastics. J. Polymer Sci. 9, 801–814.

Helm, D., 2006. Stress computation in finite thermoviscoplasticity. Int. J. Plast. 22, 1699–1727.

Kolupaev, V.A., 2006. Dreidimensionales Kriechverhalten von Bauteilen aus unverstärkten Thermoplasten. Dissertation, Halle-Wittenberg.

Lee, E.H., 1969. Elastic–plastic deformation at finite strains. J. Appl. Mech. 36, 1–6.

Lemaitre, J., Chaboche, J.L., 1990. Mechanics of Solid Materials. Cambridge University Press, Cambridge.

Mahnken, R., 1999. Aspects on the finite-element implementation of the Gurson model including parameter identification. Int. J. Plastics 15 (11), 1111–1137.

Mahnken, R., 2000. A comprehensive study of a multiplicative elastoplasticity model coupled to damage including parameter identification. Comp. Struct. 74 (2), 179–200.

Mahnken, R., 2003. Creep simulation of asymmetric effects by use of stress mode dependent weighting functions. Int. J. Solids Struct. 40, 6189–6209.

Mahnken, R., 2005a. Void growth in finite deformation elasto-plasticity due to hydrostatic stress states. Comput. Methods Appl. Mech. Eng. 194, 3689–3709.

Mahnken, R., 2005b. Creep simulation of asymmetric effects at large strains by stress mode decomposition. Comput. Methods Appl. Mech. Eng. 194, 4221–4243.

Marsden, J.E., Hughes, T.J.R., 1993. Mathematical Foundations of Elasticity. Dover Publications, New York.

Miehe, C., 1994. On the representation of Prandlt–Reuss tensors within the framework of multiplicative elastoplasticity. Int. J. Plast. 10 (6), 609–621.

Poirier, J.P., 1985. Creep of Crystals, High-Temperature Deformation Processes in Metals, Ceramics and Minerals. Cambridge University Press, Cambridge.

Potente, H., Karger, O., Fiegler, G., 2002. Laser and microwave welding—the applicability of new process principles. Macromol. Mater. Eng. 287 (11), 734–744.

Potente, H., Fiegler, G., Haferkamp, H., Fargas, M., von Busse, A., Bunte, J., 2006. An approach to model the melt displacement and temperature profiles during the laser through-transmission welding of thermoplastics. Polymer Eng. Sci., 1565–1575. doi:10.1002/pen.

Potente, H., Wilke, L., Ridder, H., Mahnken, R., Shaban, A., 2008. Simulation of the residual stresses in the contour laser welding of thermoplastics. Polymer Eng. Sci. 48 (4), 767–773. doi:10.1002/pen.20999.

Rice, J.R., 1970. On the structure of stress–strain relations for time-dependent plastic deformations in metals. ASME J. Appl. Mech. 37, 728–737.

Shaban, A., Mahnken, R., Wilke, L., Potente, H., Ridder, H., 2007. Simulation of rate dependent plasticity for polymers with asymmetric effects. Int. J. Solids Struct. 44, 6148–6162.

Simo, J., 1988. A framework for finite strain elastoplasticity based on maximum plastic dissipation and the multiplicative decomposition, Part I: continuum formulation. Comput. Methods Appl. Mech. Eng. 66, 199–219.

Simo, J.C., 1992. Algorithms for static and dynamic multiplicative plasticity that preserve the classical return mapping schemes of the infinitesimal theory. Comput. Methods Appl. Mech. Eng. 99, 61–112.

Simo, J., Pister, K., 1984. Remarks on rate constitutive equations for finite deformation problems. Comput. Methods Appl. Mech. Eng. 46, 201–215.

Simo, J., Taylor, R., Pister, K., 1985. Variational and projection methods for the volume constraint in finite deformation elasto-plasticity. Comput. Methods Appl. Mech. Eng. 51, 177–208.

Simo, J.C., Hughes, T.J.R., 1998. Computational Inelasticity, Interdisciplinary Applied Mathematics, Mechanics and Materials, vol. 7. Springer-Verlag.

Spitzig, W.A., Sober, R.J., Richmond, O., 1975. Pressure dependence of yielding and associated volume expansion in tempered martensite. Acta Metallurgica 23, 885–893.

Spitzig, W.A., Richmond, O., 1979. Effect of hydrostatic pressure on the deformation behavior of polyethylene and polycarbonate in tension and in compression. Polymer Eng. Sci. 19 (16), 1129–1139.

Steinmann, P., Miehe, C., Stein, E., 1993. Comparison of different finite deformation inelastic damage models within multiplicative plasticity for ductile materials. Int. J. Comp. Mech. 13, 458–474.